Spring 5-1-2010

Production and In Vitro Investigation of Vitamin B12-Based Bioprobes

Amy Rabideau

1 Current Cancer Diagnostics

1.1 Cancer in the U.S.

The American Cancer Society (ACS) recently estimated 562,000 American deaths were due to cancer in 2009.[i] Behind heart disease, cancer is the second-most common cause of death in the U.S; it is responsible for about one in every four American deaths. In the same report, the ACS reported that there were 1.48 million new cancer cases diagnosed in the U.S. in 2009—all with varying prognoses from early (stage I) to advanced (stage IV).[i] In the past three decades, the prognoses for 5-year survival across patients diagnosed with cancers have improved from 50 to 66%.[i] These statistics reflect progress in early diagnosis and improved treatments. However, given different treatment protocols, concomitant illnesses, and biological differences among individuals, the survival rate for one in every three cancer patients remains at less than five years.

1.2 Cancer

Cancer, also called malignant neoplasm, can develop from most cell types in the human body and is characterized by unrestrained proliferation, invasion of normal tissues, and possible metastasis to other organs. It is known to arise from changes in the genome sequences of specific cells, such as DNA mutations or abnormal gene formations.[ii] DNA base mutations include substitutions, insertions or deletions, and rearrangements due to environmental factors or viral infections, such as UV radiation[iii] and the human papilloma virus[iv]. Cancer accounts for more than 100 distinct diseases, each with varying risk factors and epidemiologies. Each type is considered to originate from a common pathogenic origin and follow

an evolutionary process.[v] The cancer genome has evolved to acquire genetic variations by random mutations and natural selection based on phenotypic advantages. Recently, scientists have begun working to sequence the cancer genome to determine the stomatically mutated genes and driver mutations that contribute to cancer development.[vi] Research on the cancer genome will help develop new diagnostic and treatment methods for cancer with the goal of diagnosing cancer sooner and with better prognoses.

1.2.1 Breast Cancer

According to the ACS Cancer Facts & Figures 2009 report, aside from skin cancer, breast cancer is the most frequently diagnosed cancer in women.[i] Mutations in specific genes have been attributed to predisposition of breast cancer. Wooster *et al*. identified the second known breast cancer susceptibility gene, BRCA2, which accounts for inherited risk for developing breast cancer. Six mutations identified in the BRCA2 gene were found to cause serious disruptions in the open reading frame, thereby increasing a person's susceptibility of developing the disease.[vii] While the risk of developing breast cancer is increased by genetic history, risk factors include obesity after menopause, the use of menopause hormone therapy (MHT), and high-dose radiation to the chest during a medical procedure.[i] Breast cancer is commonly detected using a type of X-ray scanning called mammography to look for abnormalities, such as masses or microcalcifications. Today, mammography can detect about 80-90% of breast cancers in women without symptoms.[i]

In 2007, the ACS published a set of guidelines for the use of magnetic

resonance imaging (MRI) to screen for breast cancer in patients with known susceptibility, such as those with BRAC1 or BRCA2 gene mutations or a history of Hodgkin disease treatment. Since mammography is less sensitive than MRI imaging, MRI screenings may be used to detect cancer at an earlier stage in high-risk patients. MRI uses magnetic fields to produce two-dimensional images of internal organs and tissues based on the contrast of different materials, such as fat or muscle. To achieve high sensitivity and reliable detection in MRI screenings, gadolinium-based contrast agents are injected intravenously. With inconsistent reports of specificity, numerous MRI scans must be taken after the contrast agent has been injected to distinguish between benign conditions and malignant lesions.[viii] Saslow *et al.* found that the specificity of MRI screening was significantly lower than that of mammography, as evidenced by the call-back rates for additional imaging.[ix] Although MRI imaging has higher sensitivity than mammography (or X-ray scanning) for early detection of breast cancer, a more target-specific contrast agent is necessary to increase the specificity of screening for breast cancer.

2 Medicinal Application of Imaging Agents

2.1 Medical Imaging

According to the National Institutes of Health (NIH), medical imaging refers to the process of scanning a human or animal to find clues about a medical condition. Advances in imaging from X-rays to positron emission tomography (PET) scans have made it possible to study the body using minimally- to

noninvasive techniques. Higher spatial resolutions and the development of imaging agents have made it possible for physicians and scientists to image live subjects in real time and with reliable results.

Today, the field of molecular imaging is growing exponentially. The ability to *see* specific molecular targets *in vivo* has the potential for imaging drug distribution, target binding, and even receptor expression. As the field continues to grow, the development of highly sensitive, target-specific imaging agents will push the boundaries of diagnostic medicine for earlier disease diagnoses and greater diagnostic confidence.

MRI was developed in the mid-20th century and then applied for medicinal uses in 1977.[x] Simply stated, MRI is a noninvasive procedure that uses radiowaves in the presence of a magnetic field to obtain information about internal organs and tissues. The two-dimensional representation scans are taken based on the relaxation rates of hydrogen nuclei in water contained in the tissues. These scans are typically used for producing anatomical images for the differentiation between normal and diseased tissues.

X-ray computed tomography (CT) scanning involves the passage of X-rays through different types of tissue. The angles at which the X-rays are deflected and absorbed are measured to obtain a three-dimensional image based on a collection of two-dimensional images around a single axis of rotation. CT scans are commonly used for studying skeletal structures and the lungs.

PET scanning is a type of nuclear imaging that requires the administration of an imaging agent containing a radioactive element, such as fluorine-18, carbon-

11, or oxygen-15. This technique indirectly detects γ rays that result from the positron emission associated with radioisotope decay. As the radioisotopes decay, a positron is released, which subsequently collides with an electron, producing a γ ray. Similar to CT scan analysis, PET images are compiled and reconstructed by computers to give anatomic and metabolic information. PET scanning is a versatile imaging technique that can scan various parts of the body using different types of drugs and radioisotopes. Single-positron emission computed tomography (SPECT) is an imaging technique similar to PET scanning; however, it directly detects γ rays from a γ-emitting radioisotope, such as technetium-99m or indium-111. Although CT and MRI scanning still provide greater resolution in imaging, PET and SPECT scanning allow for greater sensitivity with targeting agents.

2.2 Metal-Based Bioprobes

2.2.1 Transition Metals

The radioisotopes of technetium (^{99m}Tc) and rhenium (^{188}Re) are commonly used in diagnostic and therapeutic agents for their physical properties, including long half-lives and stable oxidation states. The easiest method for delivering these radioisotopes is by chelation to bifunctional ligands, which bind both the radioactive metal and a targeting agent.

Both technetium and rhenium are members of group 7 on the Periodic Table and therefore have similar physical properties. The fluorescent ^{186}Re(I) is used *in vitro* to test the efficacy of ligands and for direct translation to radioactive ^{99m}Tc to be used *in vivo*. Although technetium does not have any stable isotopes, it is commonly used as a radioisotope in diagnostic nuclear medicine as the

metastable isomer of ^{99}Tc, ^{99m}Tc. ^{99m}Tc can be obtained by a generator system applying the β decay of ^{99}Mo. The metastable isotope is a γ-emitter and has a half-life of 6 h, which is optimal for diagnostic medicine. As a β-emitter, ^{188}Re has the potential to be used as a therapeutic agent for treating solid tumors.[xi]

2.2.2 Lanthanides

The use of lanthanides in contrast agents has been explored in MRI imaging to increase the sensitivity of MRI in comparison to PET and SPECT. Although PET and SPECT are very sensitive types of imaging, MRI tends to be favored because is it less expensive and less time-consuming. To enhance MRI sensitivity, approximately 35% of MRI exams are performed with contrast agents, including those used for imaging breast cancer. Since MRI scans measure the relaxation of protons in water, contrast agents that are thermodynamically and kinetically stable enhance the relaxation of water protons in the body. Low molecular weight gadolinium(III)-based drugs are the most predominant contrast agents in MRI imaging today due to the metal's paramagnetic state consisting of seven unpaired f electrons and its ability to be 8-10 coordinate. Chelating ligands of the gadolinium-based contrast agents include the highly stable polyaminocarboxylate motifs, such as 1,4,7,10-tetraazacyclododecane-*N,N′,N″,N‴*-tetraacetic acid (DOTA), which is known as Dotarem® (Figure 1) in clinical use. DOTA is a stable lanthanide chelate because of its tetra-aza cycle and carboxylic acid "arms," which provide eight total sites for metal coordination. The addition of a water molecule fills in the ninth coordination site in an aqueous solution. Europium(II) is used in redox responsive contrast agents because it is

isoelectronic to Gd(III). Today, scientists are working toward developing new contrast agents that are more target-specific and facilitate higher sensitivity in tissue analysis.

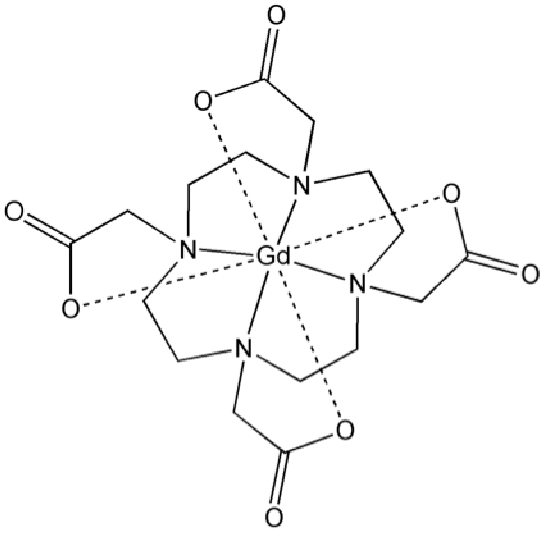

Figure 1. GdDOTA, or Dotarem®, is currently used as a contrast agent for MRI.

Fluorescent lanthanide(III) compounds are currently being designed for medical imaging. As paramagnetic metals, europium(III) and terbium(III) serve as effective fluorescent species depending on the chelating ligand. Eu(III)- and Tb(III)-based fluorescent analogues can be used to explore binding affinities of ligands used for gadolinium-based contrast agents with transport proteins, such as human serum albumin (HSA). According to a study by Hamblin *et al*., the increase in emission intensity of a binaphthyl chromophore containing Eu(III) was due to the efficient energy transfer from this ligand to europium in the presence of HSA.[xii] This study demonstrated that lanthanide-binding ligands can be tailored to bind transport proteins, used as effective bioprobes for imaging, and can be directly translated to use as gadolinium-based contrast agents. The mechanism of uptake and/or targeted tissue of specific probes can also be studied using fluorescent lanthanides. Vitha *et al.* developed two lanthanide-containing and DOTA-based contrast agents containing phosphonate moieties for targeting bone, especially in

areas of newly developed bone.[xiii] The high selectivity demonstrated by these complexes indicates their potential as bone tumor diagnostic agents.

Eu(III) and Tb(III) possess unique fluorescent properties in aqueous solutions including long fluorescence lifetimes (longer than common organic fluorophores), large Stokes' shifts, and multiple sharp emission peaks. Both ions also retain their fluorescent properties when chelated to ligands.[xiv] McMahon *et al*. explored the use of a supramolecular Eu(III) complex as a bioprobe for selective imaging of microcracks in bones often caused by constant stress due to medical conditions such as osteoporosis. The presented cyclen-based bioprobe was found to selectively bind to bone in exposed calcium(II) sites. Emissions were observed at 580, 595, 616, 655, and 701 nm in aqueous buffer at pH 7.4 upon excitation at 282 nm.[xv] Another cyclen-based Tb(III) bioprobe was developed by Bornhop *et al.* to detect early-stage oral cancer lesions using a hamster model *in vivo*.[xvi] Four emission peaks between 490 and 620 nm were observed when the contrast agent is excited at 260 nm. The incorporation of Eu(III) and Tb(III) in bioprobes holds extraordinary potential for the development of target-specific bioprobes. The ligands, through which the metal ions are chelated, provide reactive sites for conjugation of target-specific substrates.

2.3 Biocompatibilty of Bioprobes

When considering *in vivo* applications of bioprobes such as the transition- or lanthanide-based systems, biocompatibility must be taken into account. Requirements for these bioprobes include solubility and stability at physiological conditions, low toxicity, and target specificity. For MRI contrast agents, at least

one water molecule must be bound to the metal center with rapid solvent exchange to affect the relaxation times of the protons.

The use of metals for *in vivo* imaging in SPECT scanning poses a problem with regard to heavy metal toxicity. The incorporation of strong metal-chelating ligands, including cyclen and its conjugated derivatives allow the *in vivo* use of metals in bioprobes, with decreased toxic effects. In terms of toxicity, ^{99m}Tc decays to the stable ^{99}Tc form, which the body may readily excrete. Lanthanide-based drugs are excreted from the body by the kidneys before the metal ions can react with essential anions and cations in the blood.[xvii] The disadvantage of using the current lanthanide-based contrast agents is the UV excitation wavelength required to observe fluorescence is in the visible region. Using UV light *in vivo* may cause radical formation and DNA damage in the patient. The metal-based bioprobes described in this project were developed with toxicity, solubility, and target specificity in mind. Our goal for the project was to develop bioprobes with increased specificity for certain cancer cell types to help physicians diagnose cancer early and reliably, for optimal patient care and higher survival rates.

2.4 Targeting Vitamin Receptors

In order to achieve target-specific delivery of imaging or therapeutic agents for the diagnosis and treatment of cancer, genetic markers overexpressed on the surface of the tumor cells and not on normal cells must be identified. Target-specific bioprobes and therapeutics help eliminate the cytotoxic effects, such as hair loss and immunosuppression, associated with nontarget specific drugs, which tend to kill both malignant and healthy tissues. These undesirable

side effects may be avoided by utilizing a drug carrier in the form of an essential compound, such as a cofactor whose corresponding receptor is overexpressed by certain cancer cells. Recently, scientists have utilized vitamin B_{12} (B_{12}) as a drug carrier because many cancer cell types, including breast cancer, have been shown to overexpress certain B_{12} receptors (i.e. cubilin, megalin, and transcobalamin II).[xviii]

3 Vitamin B_{12}

3.1 Structure Description

B_{12}, also known as cobalamin, is a highly water-soluble (10.2 mg/mL) vitamin.[xix,xx] B_{12} is the only vitamin with a stable carbon-metal bond. It contains a six coordinate cobalt(III) atom, bound to (1) a variable group (the β-ligand), which is typically a cyano, hydroxyl, methyl, or adenosyl group, (2-5) a tetradentate corrin ring, and (6) a 5,6-dimethylbenzimidazole with a phosphoribose unit (the α-ligand), as represented in Figure 2. There are a variety of functional groups in B_{12} that may be utilized for conjugation, including three propionamide groups, three ethylamide groups, two hydroxyl groups off the phosphoribose unit, and the β-ligand site at the Co(III) metal center.

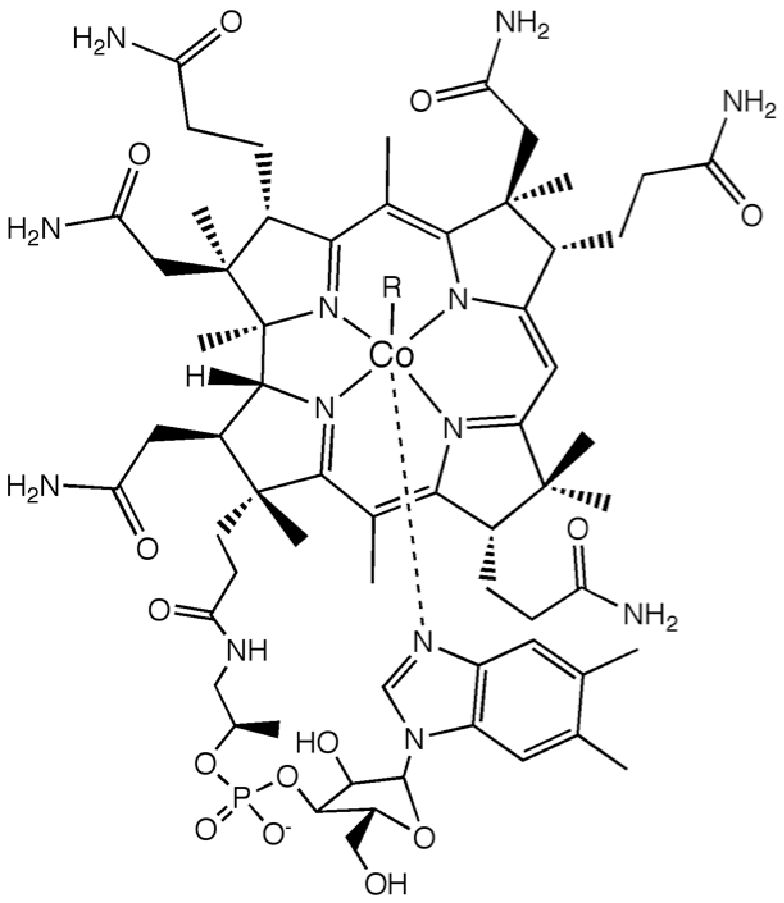

Figure 2. Structure of vitamin B_{12} (also known as cobalamin) contains a Co(III) bound to a variable group (R = methyl or adenosyl in biochemical form), a tetradentate corrin ring, and a 5,6-dimethylbenzimidazole with a phosphoribose unit.

3.2 Uptake Pathway

Despite its significance in mammalian cell growth, B_{12} is only produced by bacteria, therefore, mammals must obtain B_{12} through the food chain or by vitamin supplementation.[xxi] Since B_{12} must be taken in through the diet, a selective uptake pathway has evolved in mammals for the absorption of B_{12}.

The complex B_{12} uptake pathway includes three known transport proteins, intrinsic factor (IF), transcobalamin II (TCII), and haptocorrin (HC or TCI) and three receptors, cubilin, megalin, and TCII receptor. As represented in Figure 3,

once B_{12} is ingested, it is bound to haptocorrin, a corrinoid-binding protein and transported through the stomach, protected from the acidic environment. Once HC-B_{12} is released from the stomach, it is released from HC in the intestinal lumen and sequestered by a second protein IF (secreted by the gastric mucosa and the pancreas). The IF-B_{12} complex is transported through the intestine to the proximal ileum, where it is taken up into an enterocyte by receptor-mediated endocytosis via the cubilin receptor, anchored by the transmembrane protein, megalin. Following endocytosis, the cubilin-bound IF-B_{12} is encapsulated by an endosome at pH = 5.5, where IF is broken down by the lysosome thereby releasing B_{12}. The third transport protein TCII then binds B_{12} to be shuttled through the blood for cellular uptake. B_{12} is taken into cells either by the TCII receptor or by the megalin receptor, which both can bind B_{12}-bound TCII (holo-TCII). According to Wuerges *et al.*, approximately 25% of B_{12} binds to TCII to form holo-TCII, while the remaining B_{12} recirculates bound to HC, which is taken up and stored in hepatocytes.[xxii] Upon receptor-mediated endocytosis of holo-TCII in a cell requiring B_{12}, the acidic environment of the endosome causes B_{12} to be released. Once the endosome is broken down by the lysosome and B_{12} is released, it is subsequently methylated or adenosylated for use by the cell.

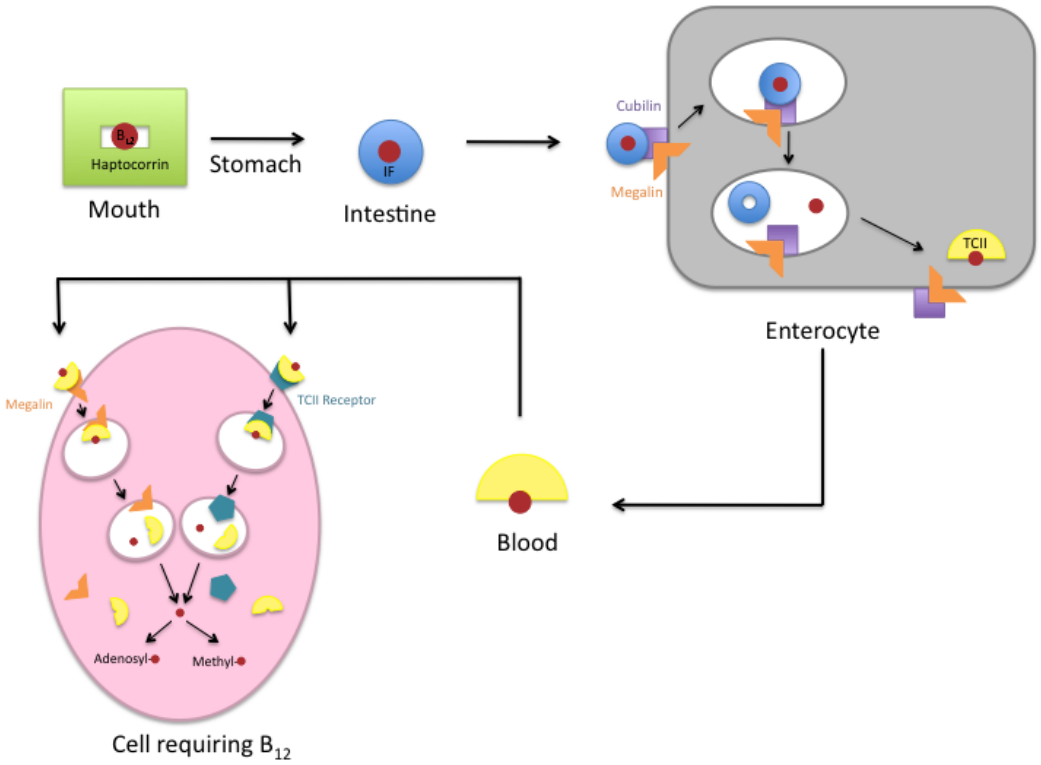

Figure 3. Uptake pathway of B_{12} is complex, requiring three transport proteins and at least three cell receptors.

3.3 Function in the Body

B_{12} is an important cofactor required for certain enzymatic processes in the mitochondria, cell nucleus, and cytoplasm. Processes include the conversion of L-methylmalonyl-CoA to succinyl-CoA using L-methylmalonyl-CoA mutase and the conversion of homocysteine to methionine using methionine synthetase. By these processes, B_{12} is necessary for DNA methylation, synthesis of red blood cells, and maintenance of the nervous system.

B_{12} deficiencies may occur as a result of the lack of or minimal absorption, transportation, and/or metabolism of the vitamin. A low intracellular B_{12} concentration may lead to anemia, degeneration of nerve fibers, or permanent neurological damage, especially among infants and the elderly.[xxiii,xxiv]

4 Vitamin B_{12} in Medical Imaging

4.1 Types of Conjugates

There is a demand for B_{12} in regions of enhanced proliferation, such as in cancer cells or sites of infection. B_{12} can serve as a viable carrier molecule or "Trojan Horse" for transporting cytotoxic agents and bioprobes to specific cells in the body. The structural complexity of B_{12} provides a number of functional sites for conjugation; however, to ensure a maximal binding potential of B_{12} transport proteins, only a few sites can be derivatized and remain active. These sites include the cobalt metal center, selected amides, and the 5′ hydroxyl group of the ribose moiety.

4.1.1 Cobalt Metal Center

Scientists have created fluorescent derivatives of B_{12} by linking fluorophores to the cobalt(III) metal center. Reaction of B_{12} with respect to the cobalt metal center produces a photolabile carbon-cobalt (Co-C) bond, which must be handled in dim light. Grissom *et al.* synthesized novel B_{12} conjugates containing pendant fluorophores known as CobalaFluors for imaging B_{12} receptors on cancer cells. The fluorophore was conjugated to B_{12} through the β-ligand position of the aminopropyl group off of the cobalt metal center. Although many fluorophores experience photobleaching under direct light exposure, electronic absorption spectroscopy indicated minimal photobleaching of the CobalaFluors under mild conditions of hydrolysis.[xxv] The stability of the CobalaFluors contributes to their potential as target-specific bioprobes for

imaging B_{12} receptors. However, steric interactions may inhibit the binding of the CobalaFluors to IF and/or TCII for transport and cellular uptake.

The cyanide group of cyano-B_{12} may also be used as a bridge for two metal centers, one of which is the cobalt metal center of B_{12}. Alberto *et al*. used the *fac*-$[^{99m}Tc(CO)_3]^+$ moiety to form a Co-C-Tc bridge for production of radiopharmaceuticals.[xxvi] Biological applications of the radioactive B_{12} bioprobe are contingent on the compound's stability and affinity for the B_{12} transport proteins.[xxvi] Binding studies of the conjugate with the different B_{12} transport proteins will reveal its potential as a bioprobe for cancer cells.

4.1.2 Amide

Modification of the amide functional groups results in varying TCII binding potentials. When converted to a carboxylic acid, the modified β position has been shown to inhibit the binding of TCII to 2.6%, to form holo-TCII, thereby inhibiting the conjugate's uptake by the cell through the TCII or megalin receptors.[xxvii] Conjugation through this amide group can serve as a good control conjugate when testing intracellular fluorescence of active B_{12}-based bioprobes.

4.1.3 Ribose

Rather than derivatizing the cobalt metal center, which has potential to interact with the B_{12} transport proteins, scientists have looked to conjugate fluorophores to the 5′ hydroxyl group of the ribose moiety of B_{12}. Fedosov *et al.* conjugated a rhodamine fluorophore derivative to B_{12} through the 5′ hydroxyl group using a 1,1-dicarbonyl-di-(1,2,4-triazole) (CDT) coupling agent. The derivative was then bound to two B_{12} transport proteins, TCII and IF for binding

kinetic studies.[xxviii]

4.2 Drug Delivery System

This project looked at the conjugation of a bifunctional ligand to B_{12} through the 5′ hydroxyl group of the ribose moiety to optimize its uptake by cell receptors via B_{12} transport proteins. It followed a typical metal-based drug design (Figure 4) consisting of the target molecule (B_{12}) linked to a bifunctional ligand, which was used to chelate a metal ion such as $^{186/188}$Re, ^{99m}Tc, Eu, or Tb.

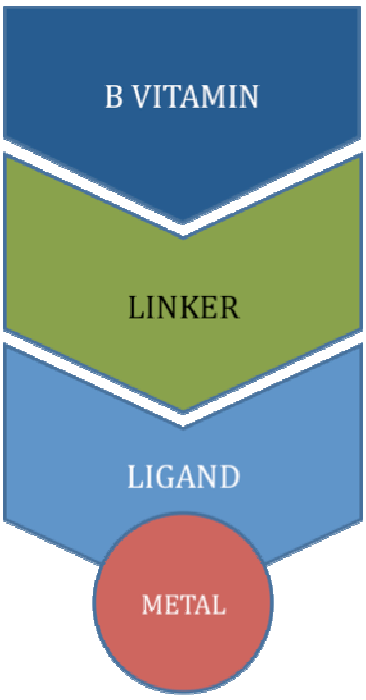

Figure 4. Bifunctional drug contains a target molecule conjugated through a ligand to a metal ion.

5 B_{12}-ReBQBA

This project was inspired by the limited tissue expression of cubilin and its putative importance for cancer cell growth. The specific aim for this project was to exploit the use of the cubilin receptor for delivery of a B_{12} conjugate using the B_{12} transport protein IF. Cubilin was targeted for the selective delivery and accumulation of a new bioprobe, a B_{12} conjugate of rhenium BQBA (B_{12}-ReBQBA), in the cubilin expressing placental choriocarcinoma BeWo cell line. Receptor-mediated endocytosis was utilized as a transport mechanism for facilitating cellular entry of a rhenium fluorescent probe tethered to B_{12}. *In vitro* cytotoxicity assays and uptake studies via fluorescent confocal microscopy were conducted on two different cell lines: human placental choriocarcinoma (BeWo)

(cubilin (+)) and Chinese hamster ovary (CHO) cells (cubilin (-)).

5.1 Synthesis

5.1.1 ReBQBA

A *N*,*N*-bis(quinolin-2-ylmethyl)butane-1,4-diamine (BQBA) ligand was synthesized as a bifunctional chelator, as shown in Figure 5, with a site for the coordination of a metal center *and* a terminal amine for further conjugation. BQBA was initially synthesized by two successive reductive aminations. Bisquinoline-2-carboxaldehyde (100 mg, 0.636 mmol) was reacted with *N*-boc-1,4-diaminobutane (121.7 μL, 0.636 mmol) in dichloroethane (DCE) (5 mL) at room temperature for 1 h. The reaction was cooled to 0 °C then reduced using sodium triacetoxyborohydride (161 mg, 0.763 mmol) for 1 h. This procedure was repeated for the second equivalent of bisquinoline-2-carboxaldehyde (100 mg, 0.636 mmol). The reaction solution was washed three times with water (10 mL) and once with 3.5 M sodium chloride (10 mL). The organic layer was dried over sodium sulfate. The solvent was removed *in vacuo* to yield a dark red solid. The reaction product was extracted using a 1:1 ethylacetate/hexane solution.

Purification of the reaction product was achieved by dissolving the boc-BQBA complex in concentrated diethyl ether then precipitating the purified product at -20 °C. Purity of the compound was confirmed by proton NMR and electrospray ionization mass spectrometry (ESI-MS). The ^{1}H NMR of boc-BQBA was taken in deuterated chloroform at 300 MHz. ^{1}H NMR peaks included δ = 8.135 (2H, d), 8.060 (2H, d), 7.790 (2H, d), 7.700 (4H, m), 7.510 (2H, m), 4.014 (4H, s), 3.050 (2H, m), 2.637 (2H, t), 1.60-1.80 (4H, m), and 1.20-1.50 (9H, m).

The mass spectrum using ESI-MS included a $[M + H]^+$ peak at 491.25 *m/z* with an isotopic pattern indicative of boc-BQBA, $C_{29}H_{34}N_4O_2$ (M = 470.27 g/mol). The boc protecting group was removed by adding 10% trifluoroacetic acid (TFA) in chloroform and mixing overnight. The deprotected BQBA product was confirmed by ^{1}H NMR and ESI-MS.

The bifunctional chelate was labeled with rhenium(I) tricarbonyl using a molar equivalent of the rheunium metal precursor, $[Re(H_2O)_3(CO)_3]Br$, in methanol and stirred at 60 °C for 3 h. Upon conjugation to rhenium, the ^{1}H NMR in deuterated chloroform indicated a downfield shift of the aromatic and bridging CH_2 protons, adjacent to the rhenium metal core. Yield was quantitative.

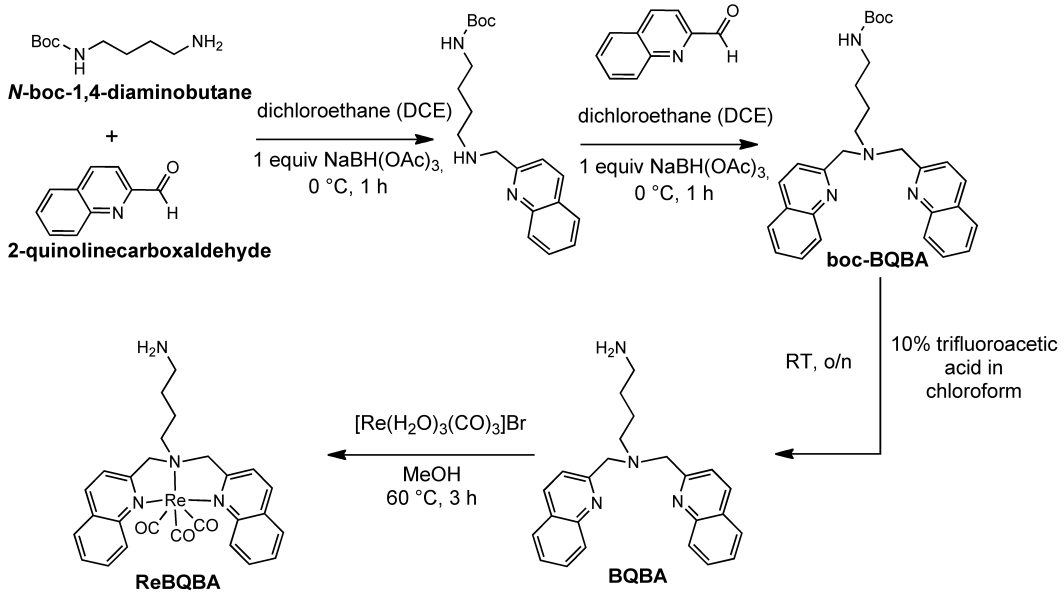

Figure 5. Synthetic scheme for ReBQBA.

5.1.2 B_{12}-ReBQBA

In order to target the cubilin receptor using IF, the B_{12}-ReBQBA conjugate, shown in Figure 6, was designed to not interfere with the IF-cubilin binding. This was accomplished by attaching the ReBQBA ligand to B_{12} through

the 5′-hydroxyl group of the ribose moiety of B_{12}. The cyano derivative of B_{12} (cyano-B_{12}) was used for conjugation to minimize potential side reactions of the photolabile cobalt-carbon bond.

The 5′ hydroxyl group of cyano-B_{12} (25.0 mg, 0.0369 mmol) was activated with 1.2 equiv of 1,1′-carboyl-di-(1,2,4-triazole) (CDT) (4.40 mg, 0.0244 mmol) in 3 mL of dry dimethyl sulfoxide (DMSO) at 60 °C over 30 min under inert $N_{2\,(g)}$. The ReBQBA ligand (14.2 mg, 0.0221 mmol) previously dissolved in 2 mL of DMSO was added dropwise to the CDT-activated B_{12}. The reaction solution was stirred under $N_{2\,(g)}$ for 6 h at RT. After 6 h, the reaction product was precipitated out of DMSO using a 4:1 diethyl ether/acetone solution. A deep red precipitate was centrifuged at 3452 *g* for 10 min. The red precipitate was dried under vacuum overnight prior to being redissolved for purification.

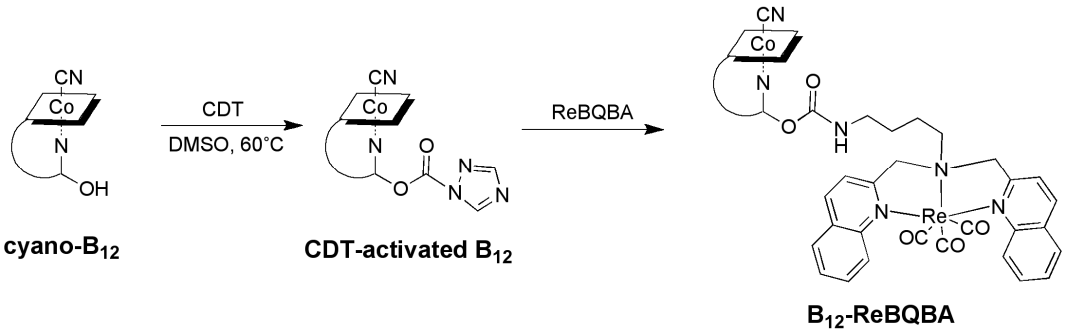

Figure 6. Synthetic scheme for B_{12}-ReBQBA.

The deep red precipitate was redissolved in a 4:1 water/acetonitrile solution and subsequently purified via reverse phase high performance liquid chromatography (RP-HPLC). The crude B_{12}-ReBQBA sample was purified on a Zorbax C_{18} semipreparative column (250 mm x 9.4 mm) at a flow rate of 2.0 mL/min. Solvents for elution included (A) water (0.1% TFA) and (B) acetonitrile

(0.1% TFA). The gradient was (1) 30 – 50% B over 16 min and (2) 50 – 100 % B over 5 min. Under this method, the retention time of B_{12}-ReBQBA was 13.7 min. The percent yield was approximately 12–17%.

Purified B_{12}-ReBQBA was confirmed via ^{1}H NMR, matrix assisted laser desorption ionization time-of-flight mass spectrometry (MALDI-TOF/MS), and inductively coupled plasma (ICP).

A ^{1}H NMR spectroscopic analysis of B_{12}-ReBQBA confirmed the proposed structure. Upon conjugation to B_{12}, the ^{1}H NMR taken in deuterium oxide at 300 MHz indicated a downfield shift of the ribose aromatic protons, adjacent to the ReBQBA.

The MALDI-TOF/MS of B_{12}-ReBQBA displayed three sets of peaks with the parent peak at 2022.3 *m/z*, consistent with the theoretical molecular mass of $[M^{+}]$ = 2022.1 for $C_{91}H_{112}CoN_{12}O_{12}PRe$. The isotopic pattern of this parent peak was consistent with that of the theoretical pattern of B_{12}-ReBQBA. Fragments consisted of the base peak at 1994.9 *m/z* determined to be $[M^{+} – CO]$ and a set of peaks around 1966.9 m/z determined to be $[M^{+} – 2CO]$.

ICP results indicated the presence of rhenium. The carbamate linker from B_{12} to ReBQBA was proven to be stable for at least 24 h between pH 5.5 and pH 7.4 by reverse phase (RP)-HPLC.

5.2 Binding to Intrinsic Factor

IF was bound to B_{12}-ReBQBA prior to *in vitro* cell testing to ensure cellular uptake by the cubilin receptor. Binding of IF to B_{12}-ReBQBA was monitored by electronic absorption spectroscopy, Figure 7. IF was aliquoted into

a solution containing B_{12}-ReBQBA in phosphate buffered saline (PBS). An increase in absorption intensity was observed, indicating binding of IF to B_{12} because the symmetry of the corrin ring of B_{12} was reduced. Saturation of IF was indicated by a constant absorbance intensity with additional IF aliquots.

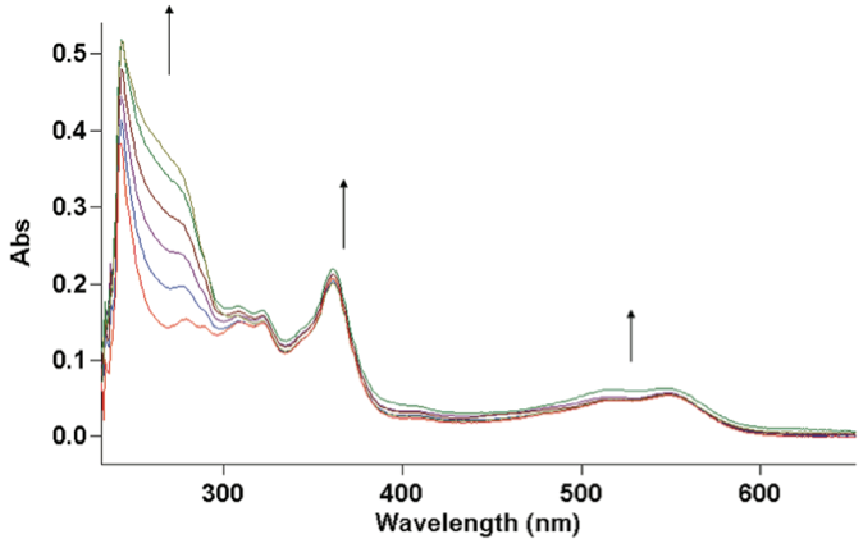

Figure 7. Electronic absorption spectroscopy was used to follow IF binding to B_{12}-ReBQBA.

5.3 Cytotoxicity Studies

Conjugates were tested against BeWo and CHO cell lines to determine the IC_{50} value (the concentration at which the conjugates inhibit 50% of cell growth). The BeWo and CHO cells were cultured at 90% confluence and inoculated into a 96-well plate at ~8000 cells/well. The cells were incubated for 24 h to allow for cell adherence. Stock solutions of BQBA, ReBQBA, B_{12}-ReBQBA, and IF-B_{12}-ReBQBA were prepared with RPMI 1640 media. Ten-fold dilutions of the drugs (100 µL) were added to the cells and incubated for 6 h. The drug solutions were removed from the plates then washed with media to remove excess drugs. A 10% Cell Counting Kit-8 (CCK-8) dye solution was prepared using RPMI 1640 media

enriched with fetal bovine serum and penicillin streptomycin. CCK-8 dye (100 µL) was added to the plates and incubated for 24 h. The calculated IC_{50} values for BeWo and CHO cells were tabulated in Table 1.

Table 1. IC_{50} Values (mM) Calculated for BeWo and CHO Cells after 6 hr of Drug Exposure

	IC_{50} (mM)	
Drug	**BeWo**	**CHO**
BQBA	> 5.000	2.979 ± 0.210
ReBQBA	0.376 ± 0.028	2.627 ± 0.280
B_{12}-ReBQBA	3.180 ± 0.258	> 5.000
IF-B_{12}-ReBQBA	1.844 ± 0.478	4.860 ± 0.283

Uptake of BQBA, ReBQBA, and B_{12}-ReBQBA in the BeWo cell line was attributed to passive diffusion due to size. Additionally, the enhanced uptake of rhenium-containing drugs may be due to the positive charge of rhenium(I), which provides electrostatic interactions with membrane proteins, allowing for passive diffusion of the drugs. As demonstrated by Patillo *et al.*, the BeWo cell line has a negative transmembrane potential of about -35 mV.[xxix] IC_{50} values were used to confirm uptake of the IF-bound drug in the cubilin receptor-containing BeWo cell line, and likewise, minimal uptake of the IF-bound drug in the cubilin-lacking CHO cell line. The presence of the cubilin receptor in the BeWo cell line explains the increased toxicity of IF-B_{12}-ReBQBA. The higher IC_{50} value for the same drug in the CHO cell line is most likely due to the inability of the CHO cells to internalize the drug without the cubilin receptor.

5.4 Confocal Microscopy

Drug uptake experiments were performed using the BeWo cell line. The cells were grown in RPMI 1640 with 10% fetal bovine serum and 10% penicillin-streptomycin antibiotic. They were plated at 200,000 cells/plate. The drug, 10 µM

IF-B_{12}-ReBQBA, was added to the plates, which were then incubated for 45 min and 6 h to allow for sufficient uptake time. The drug was removed via pipet, and the cells were subsequently washed three times with RPMI 1640 and 1X PBS buffer (pH 7.4) to remove excess drug. Intracellular fluorescence was observed, as seen in Figure 8, in the BeWo cells after 45 min drug incubation. The rapid uptake of the large IF-bound drug is indicative of receptor-mediated endocytosis. Optical depth scans were taken at 1 μm/slice, showing fluorescence in the middle slices of the cell and confirming internalization of the drug after 45 min.

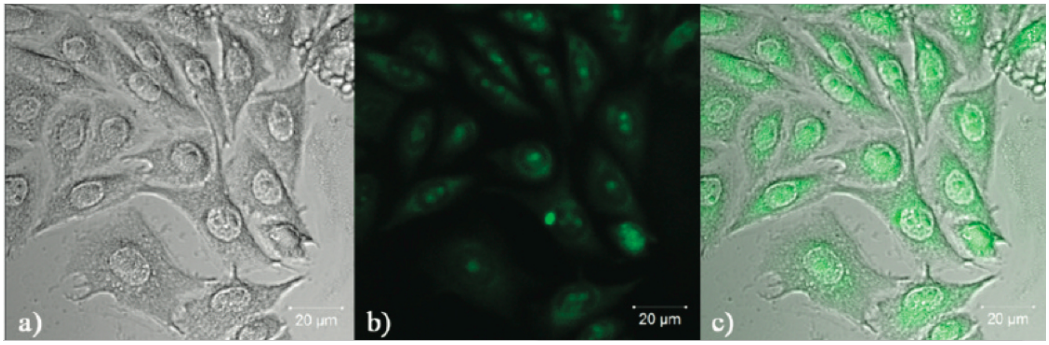

Figure 8. Cell binding and internalization of IF-B_{12}-ReBQBA after 45 min incubation with BeWo cells. Images (a) collected by a monochromatic transmitted light photomultiplier tube (TMPT-1) and (b) after excitation at 488 nm with ~560 nm emission. (c) The merged images after simultaneous scans of (a) and (b).

Receptor-mediated endocytosis of IF-B_{12}-ReBQBA into the BeWo cells was further confirmed by the internalization of a pH-sensitive cyanine dye, CypHer5E, conjugated to IF. This dye with a pKa of 7.3 fluoresces red in acidic conditions. Once this dye is internalized by receptor mediated endocytosis, it is encapsulated in an endosome, which has an acidic environment of pH ~5.5. The fluorescence from the red dye combined with the green fluorescence from the IF-B_{12}-ReBQBA drug yielded a yellow color in the merged image, Figure 9. This counterstaining experiment provides further evidence of drug uptake by cubilin-

mediated endocytosis.

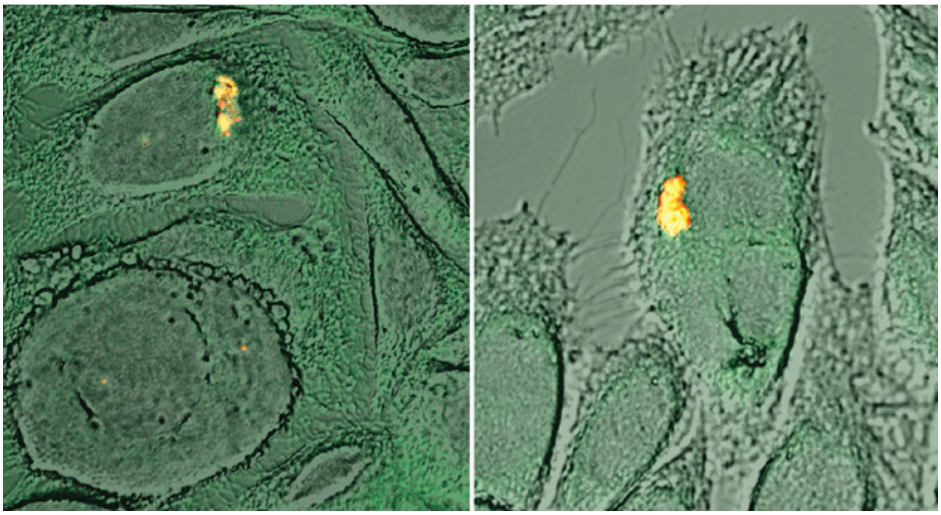

Figure 9. Receptor-mediated endocytosis was confirmed by CypHer5E endosome counterstaining.

Competitive binding studies were performed with IF-B_{12}-ReBQBA in the presence of excess free B_{12}. Excess B_{12} was added to the cells at concentrations of 100 μM and 10 mM and incubated for 5 min at room temperature. After 5 min, 10 μM IF-B_{12}-ReBQBA was added to the cells, which were then incubated for 45 min. The cells were then washed and imaged under the confocal microscope at an excitation of 488 nm. At high concentrations of free B_{12} (10 mM), cellular uptake and accumulation of IF-B_{12}-ReBQBA was inhibited.

CHO cells, which lack the cubilin receptor, were investigated for uptake of IF-B_{12}-ReBQBA as a control. Under the confocal microscope, there was no observed fluorescence of IF-B_{12}-ReBQBA in the CHO cells. This observation indicated a lack of uptake of the drug via the IF-mediated cubilin receptor.

Since propidium iodide (PI) is known to intercalate DNA and RNA, it was used as a counterstain to determine whether B_{12}-ReBQBA localizes in the nucleus. Confocal images of BeWo cells with PI, as seen in Figure 10, indicate

aggregation of B_{12}-ReBQBA in the cytosol as well as the nucleus. These images suggest that the positively charged rhenium-based drug can interact with the negatively charged DNA backbone of the cells.

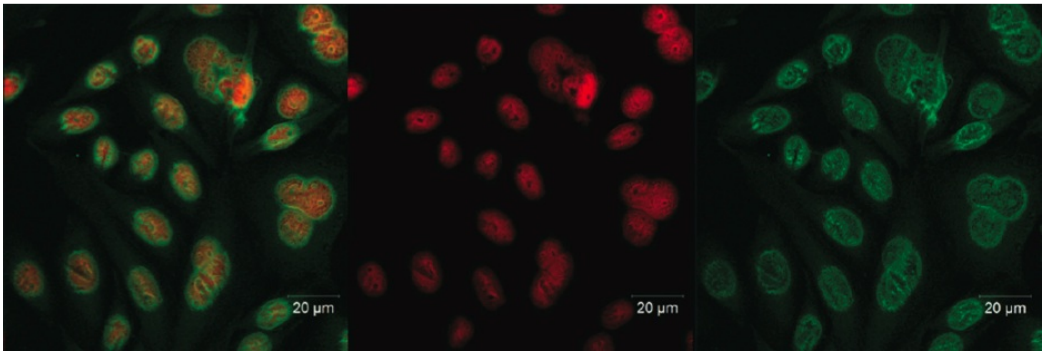

Figure 10. Propidium iodide counterstaining with IF-B_{12}-ReBQBA indicated nuclear and cytosolic drug accumulation.

5.5 siRNA Gene Knockout of Cubilin Receptor

Small interfering RNA (siRNA) transfection was used to confirm specific uptake of IF-B_{12}-ReBQBA by the cubilin receptor, as indicated by cytotoxicity assays and confocal microscopy experiments. The siRNA was used to knockdown cubilin mRNA expression in the BeWo cells. Confocal experiments showed illumination for both control and transfected cells, however at fluorescent intensities of 10-fold difference. The control had a mean intensity of 4.0, while the transfected cells had a mean intensity of 0.4. The decrease in intensity indicated a successful knockdown of the cubilin receptor. This result also provides further evidence that the IF-B_{12}-ReBQBA is taken into cells by cubilin receptor-mediated endocytosis.

5.6 Conclusions

A rhenium-based bioprobe, B_{12}-ReBQBA, was successfully synthesized, purified, characterized, and cell-tested for targeted drug delivery. The bioprobe

was found to have millimolar toxicity in placental cancer cells containing the cubilin receptor. It can also be excited at a visible wavelength to achieve emission in the visible region. Intracellular fluorescence of B_{12}-ReBQBA demonstrated the potential for IF-mediated delivery of B_{12} conjugates by the cubilin receptor for imaging cubilin-overexpressing malignancies. The bioprobe can be readily switched to a radioactive derivative containing technetium-99m for *in vivo* studies using SPECT scanning. This work was recently published in the Journal of Medicinal Chemistry.[xxx]

6 B_{12}-enDOTALn

As alternatives to gadolinium(III)-based contrast agents used in MRI imaging, europium(III)- and terbium(III)-containing bioprobes were developed as target-specific imaging agents with unique fluorescent properties. Eu(III) and Tb(III) were chelated by a bifunctional macrocycle, DOTA, which will not only coordinated the metal but was also conjugated to cyano-B_{12}. These nonradioactive B_{12} bioprobes will be tested on the T-47D breast cancer cell line, which overexpresses the TCII and HC receptors. A pancreatic cancer cell line, MIA PaCa-2, which does not express the HC receptor, will also be used to test the bioprobes.

6.1 Synthesis of B_{12}-enDOTA

An amino-terminal conjugate of cyano-B_{12} was synthesized by attaching an ethylenediamine (en) linker to the 5′-hydroxyl group of the ribose moiety of B_{12}. The en linker was used to allow for carbamate linkages to be formed instead

of weak ester bonds, which are readily hydrolyzed in aqueous environments.

The 5′ hydroxyl group of cyano-B_{12} (100.0 mg, 73.8 mmol) was activated with 1.45 equiv of CDT (17.6 mg, 107.3 mmol) in 6 mL of dry DMSO at 40 °C over 1 h under inert $N_{2\,(g)}$, as seen in Figure 11. Ethylenediamine (4.59 μL, 68.7 mmol) and triethylamine (TEA) (9.59 μL, 68.8 mmol) were diluted in 1 mL dry DMSO. The CDT-activated B_{12} was added dropwise over 30 min to the en/TEA solution. The reaction solution was stirred under $N_{2\,(g)}$ for 3 h at 40 °C. After 3 h, the reaction product was precipitated out of DMSO using a 4:1 diethyl ether/acetone solution. A deep red precipitate was spun down at 3542 *g* for 10 min. The red precipitate was dried *in vacuo* overnight prior to being reacted further.

Assuming a yield of 100% for the B_{12}-en reaction (106 mg, 73.8 mmol), the metal-chelating macrocycle DOTA was conjugated to the unpurified B_{12}-en conjugate. Given the four reactive carboxylic acid sites of DOTA, a two equivalent excess was activated to ensure that most of the B_{12}-en reacted to form the B_{12}-enDOTA monomer.

DOTA was activated using the water-soluble coupling agent 3-(ethyliminomethyleneamino)-*N,N*-dimethyl-propan-1-amine (EDC) with *N*-hydroxysulfosuccinimide (sulfo-NHS) to increase coupling efficiency. Assuming complete conjugation, the theoretical yield for B_{12}-en was calculated to be 106 mg (73.8 mmol). Two equiv of DOTA (59.4 mg, 0.147 mmol) and 2.5 equivalents of sulfo-NHS (47.9 mg, 0.221 mmol) were dissolved in 100 μM sodium phosphate (1 mL). EDC (30.9 mg, 0.162 mmol) was dissolved separately in 100 μM sodium

phosphate (50 µL) then added to the DOTA and sulfo-NHS solution for 20 min at room temperature. Upon activation, B_{12}-en dissolved in minimal 100 µM sodium phosphate (2 mL) was added to the activated DOTA. The reaction was left overnight at room temperature and purified by anion exchange (ANX) and RP-HPLC.

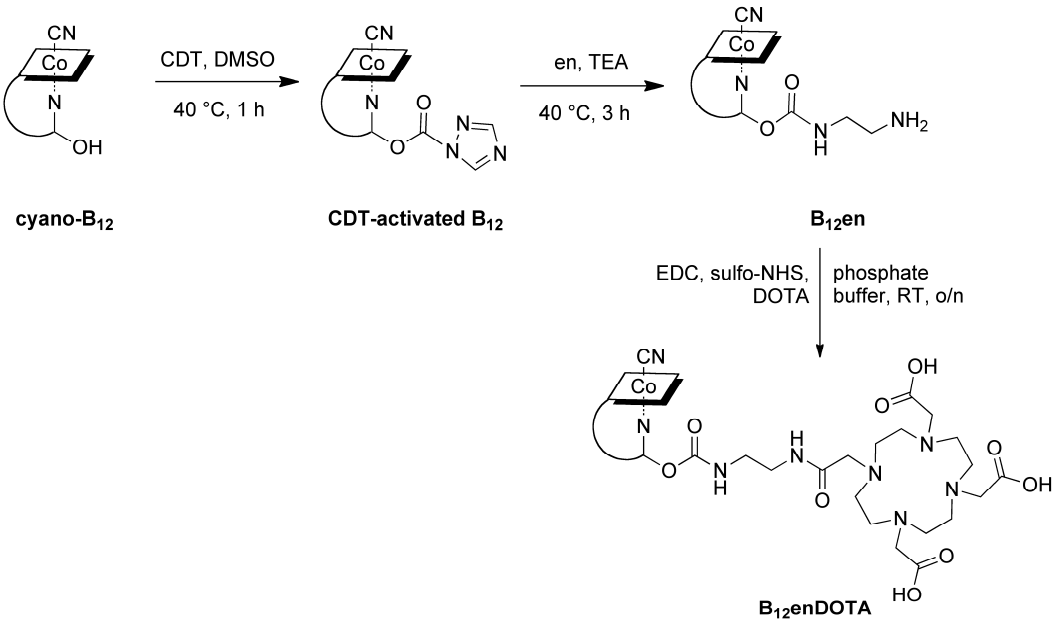

Figure 11. Synthetic scheme for B_{12}-enDOTA.

A two-step purification scheme was developed for the separation of B_{12}-enDOTA (1) from unreacted B_{12} and B_{12}-en and (2) from any B_{12}-enDOTA oligomers. The first purification was performed using a Zorbax Sax analytical anion exchange (ANX) column (4.6 mm x 250 mm) on a high performance liquid chromatograph. Solvents for elution included (A) water and (B) 0.5 M sodium chloride. At a flow rate of 1.0 mL/min, the gradient was (1) 100% A for 6 min then (2) 100 % B for 22 min. Each peak was collected and characterized by MALDI-TOF/MS. The ANX HPLC peak with a retention time of 13–14.5 min had major MALDI-TOF/MS peaks with similar isotopic patterns at 1801.7 *m/z*,

2770.1 *m/z*, and 3198.3 *m/z*, indicative of $[B_{12}\text{-enDOTA} - CN]^+$, $[B_{12}\text{-enB12} - CN]^+$, and $[B_{12}\text{-en-DOTA-enB}_{12} - CN]^+$, respectively. B_{12}-enDOTA was confirmed by mass spectrometry to elute off the column at a retention time of 13–14.5 min. However, as indicated by mass spectrometry, a second purification method was required to isolate the target product, B_{12}-enDOTA. The target peak was dried *in vacuo* then redissolved in water with 0.1% TFA to protonate the three unbound carboxylic acid arms of DOTA to form a uniform protonation state for C_{18} RP-HPLC purification.

The second purification was performed using a Zorbax C_{18} analytical column (42 mm x 10 mm) at a flow rate of 1.0 mL/min. Solvents for elution included (A) water (0.1% TFA) and (B) acetonitrile (0.1% TFA). The gradient was 10 – 20 % B over 10 min. With this method, the retention time of B_{12}-enDOTA was 7.17 min. The MALDI-TOF/MS of this HPLC peak contained a peak at 1801.7 *m/z*, consistent with the theoretical molecular mass of $[M^+]$ = 1827.9 minus the cyano group of cyano-B_{12}, $[M^+ - CN]$ = 1801.8 *m/z*. The isotopic pattern of this parent peak was consistent with that of the theoretical pattern of B_{12}-enDOTA, $C_{82}H_{120}CoN_{20}O_{22}P$, as shown in Figure 12.

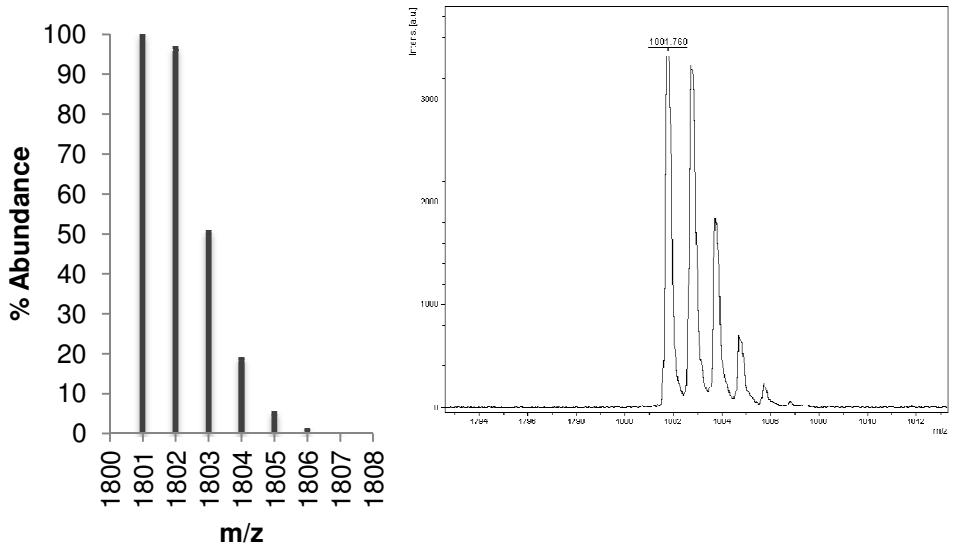

Figure 12. Theoretical (left) and experimental (right) isotopic patterns of [B_{12}-enDOTA$^+$ – CN] are equivalent.

Purity of B_{12}-enDOTA was confirmed via ^{1}H NMR and MALDI-TOF/MS. A ^{1}H NMR spectroscopic analysis of the bright red solid confirmed the proposed structure of B_{12}-enDOTA. The ^{1}H NMR was taken in deuterium oxide at 300 MHz and indicated a downfield shift of the ethylene protons of DOTA. ^{1}H NMR peaks included δ = 7.306 (1H, s), 7.126 (1H, s), 6.517 (1H, s), 6.361 (1H, s), and 6.111 (1H, s). The yield of B_{12}-enDOTA was approximately 11%.

A second peak from the HPLC had a retention time of 5.11 min. This peak was confirmed by MALDI-TOF/MS to be B_{12}-enDOTA with a proton captured within the DOTA macrocycle, 1801.1 *m/z* and multiple sodium adducts at [M^+ – CN + Na] = 1823.1, [M^+ – CN + 2Na] = 1845.1, [M^+ – CN + 3Na] = 1867.1, and [M^+ – CN + 4Na] = 1883.0 *m/z*. When heated at 65 °C, this species disappears in the HPLC, indicating the proton being driven out of DOTA or loss of a sodium adduct.

6.2 Synthesis of B12-enDOTALn

6.2.1 B12-enDOTAEu

B_{12}-enDOTA was reacted with europium(III) trifluoromethanesulfonate (Eu(III) triflate) to synthesize the bioprobe, B_{12}-enDOTAEu. Equal equivalents of B_{12}-enDOTA (3.75 mg, 2.05 μmol) and Eu(III) triflate (1.23 mg, 2.05 μmol) were refluxed at 60 °C overnight in a 1:4 water/acetonitrile solution, as in Figure 13. The reaction was monitored by RP-HPLC using the same conditions as those used to purify B_{12}-enDOTA.

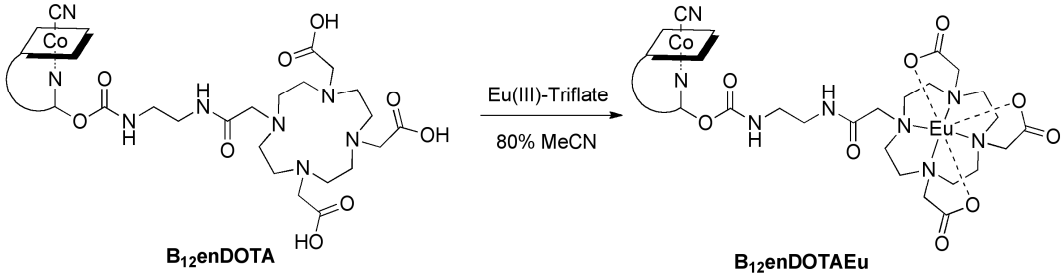

Figure 13. Synthetic scheme of B_{12}-enDOTAEu.

After 16 h, the reaction was purified by a Zorbax C_{18} analytical column (42 mm x 10 mm) at a flow rate of 1.0 mL/min using the same conditions as those used to purify B_{12}-enDOTA. The retention time for B_{12}-enDOTAEu shifted from 7.17 to 6.90 min. MALDI-TOF/MS was used to confirm the synthesis of B_{12}-enDOTAEu. A peak at 1951.0 *m/z* was indicative of $[M^+ - CN - 3H]$ and was consistent with the theoretical isotopic pattern of $C_{81}H_{118}CoN_{19}O_{22}PEu$, as shown in Figure 14. The loss of three protons indicated that the three unbound carboxylic acid arms of DOTA are deprotonated. Additionally, a sodium adduct of B_{12}-enDOTAEu with the same isotopic pattern occurred at $[M^+ - CN + Na] = 1973.0$ *m/z*.

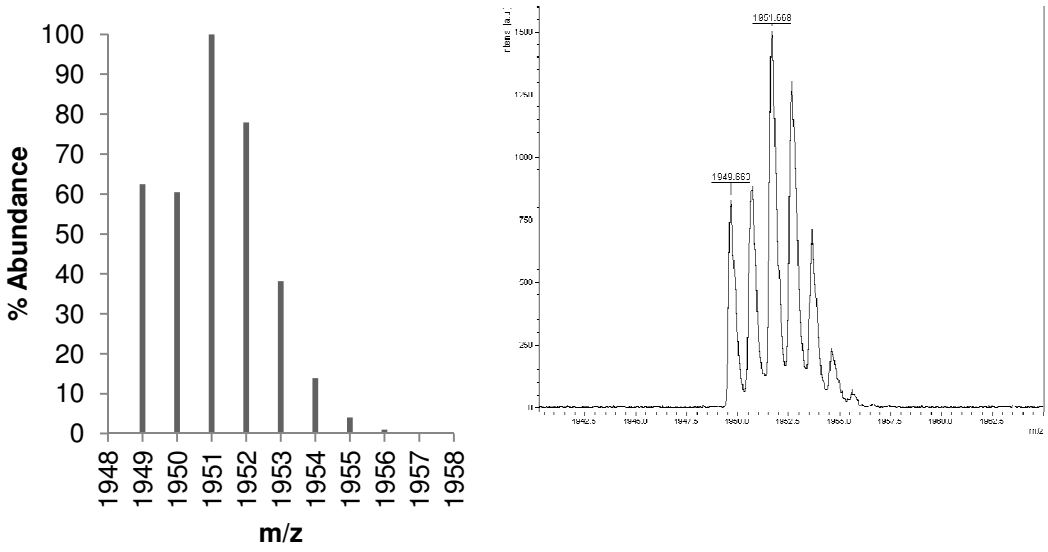

Figure 14. Theoretical (left) and experimental (right) isotopic patterns of [B_{12}-enDOTAEu^{+} – CN – 3H] are equivalent.

A ^{1}H NMR was taken of the B_{12}-enDOTAEu conjugate in D_2O at 300 MHz. ^{1}H NMR peaks included δ = 8.21 (1H, s), 6.99 (1H, s), 6.54 (2H, m), and 6.13 (1H, m). The 8.21 ppm peak is speculated to be one of the aromatic protons of the 5,6-dimethylbenzimidazole nucleotide of B_{12}. It appeared that this proton shifted downfield from its original position at 7.28 ppm (H_A, as seen in Figure 15).[xxxi] The drastic shifting of the aromatic proton adjacent to the site of conjugation and europium labeling indicates the successful conjugation of europium into DOTA. The H_B aromatic proton of the 5,6-dimethylbenzimidazole nucleotide, positioned at 7.10 ppm, appeared to have shifted upfield slightly to 6.99 ppm. The ^{1}H NMR also indicated that there was one missing B_{12} aromatic proton. It has

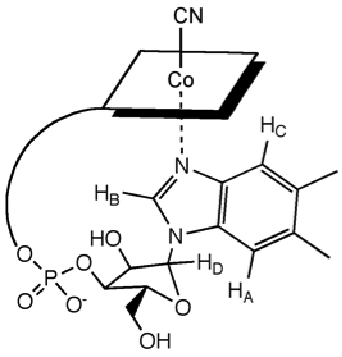

Figure 15. Protons A-D of the 5,6-dimethylbenzimidazole nucleotide of B_{12} experienced shifting in the NMR upon chelation of europium.

been speculated that the missing proton shifted to overlap the proton at 6.54 ppm. According to Brasch *et al.*, these protons are H_C and H_D, which are positioned at 6.51 and 6.36 ppm in D_2O at 25 °C, respectively.[xxxi] The fifth aromatic proton, off the corrin ring, remained undisturbed at 6.09 ppm. The yield of B_{12}-enDOTAEu was quantitative.

6.2.2 B12-enDOTATb

A similar synthetic scheme was followed for the synthesis of B_{12}-enDOTATb. B_{12}-enDOTA was reacted with terbium(III) trifluoromethanesulfonate (Tb(III) triflate) to synthesize the bioprobe, B_{12}-enDOTATb. Equal equivalents of B_{12}-enDOTA (3.75 mg, 2.05 μmol) and Tb(III) triflate (1.24 mg, 2.05 μmol) were refluxed at 60 °C overnight in a 1:4 water/acetonitrile solution, as seen in Figure 16. As with the B_{12}-enDOTAEu synthesis, the reaction was monitored by RP-HPLC using the same conditions as those used to purify B_{12}-enDOTA.

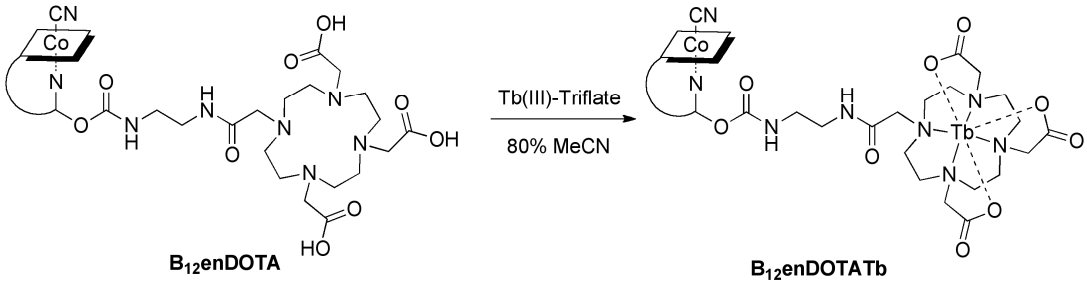

Figure 16. Synthetic scheme of B_{12}-enDOTATb

After 16 h, the reaction was purified by a Zorbax C_{18} analytical column (42 mm x 10 mm) at a flow rate of 1.0 mL/min using the same conditions as those used to purify B_{12}-enDOTA. The retention time for B_{12}-enDOTATb shifted from 7.17 to 6.89 min. MALDI-TOF/MS was used to confirm the synthesis of B_{12}-

enDOTATb. A peak at 1957.0 *m/z* was indicative of $[M^+ – CN – 3H]$ and was consistent with the theoretical isotopic pattern of $C_{81}H_{118}CoN_{19}O_{22}PTb$, as shown in Figure 17. The loss of three protons indicates that the three unbound carboxylic acid arms of DOTA are deprotonated. Similar to the europium labeling of B_{12}-enDOTA, a sodium adduct of B_{12}-enDOTATb with the same isotopic pattern occurred at $[M^+ – CN + Na] = 1979.0$ *m/z*. The yield of B_{12}-enDOTATb was quantitative.

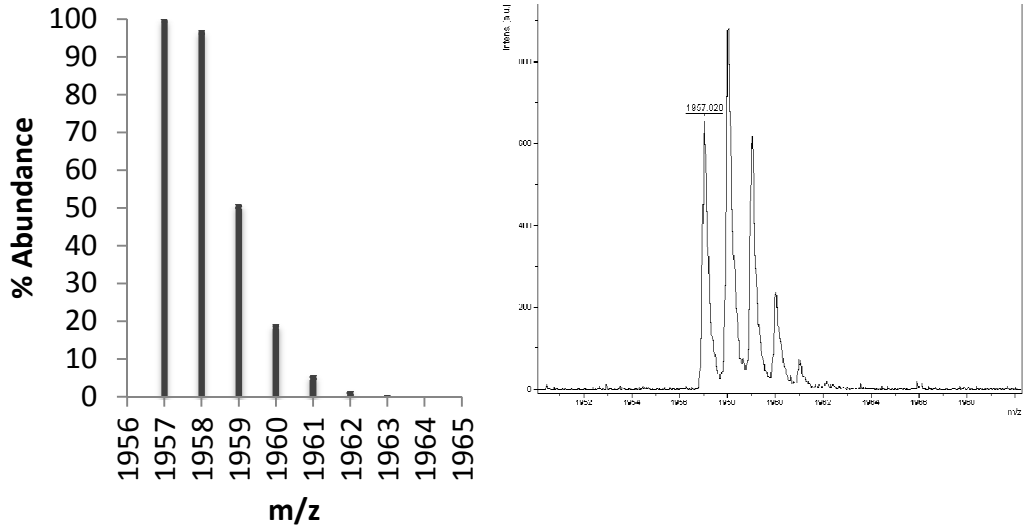

Figure 17. Theoretical (left) and experimental (right) isotopic patterns of $[B_{12}$-enDOTATb$^+ – CN – 3H]$ are equivalent.

Unlike the ^1H NMR of B_{12}-enDOTAEu, the aromatic protons in the ^1H NMR of B_{12}-enDOTATb were indistinguishable under the NMR conditions trialed. The paramagnetic character of terbium accounts for this observation.

6.3 Confocal Microscopy

The T-47D breast cancer cell line, containing both the HC and TCII receptors, will be used to test the lanthanide(III)-containing B_{12} bioprobes for *in vitro* fluorescence. The intensity of the fluorescence will be analyzed by confocal

microscopy. Preliminary confocal microscopy and two-photon imaging has indicated that a laser in the UV region (<350 nm) is required to excite the lanthanide metals chelated in the bioprobes in order to see emission in the visible region. This work is on going.

Previous research has indicated that a laser in the UV region (~282 nm) is required to excite Ln(III)DOTA, without any sensitizing substituents.[xxxii] Pandya *et al.* recently published a paper on a series of substituents that may be conjugated to the DOTA macrocycle to increase the pi bonding within the bioprobes. Possible substituents include the aza-thiaxanthone or tetraazatriphenylene chromophores.[xxxii]

7 Future Research

7.1 B_{12}-enDOTALn Imaging

Imaging of B_{12}-enDOTAEu and B_{12}-enDOTATb derivatives as well as the EuDOTA and TbDOTA control systems on the T-47D and MIA PaCa-2 cell lines will wait until we have access to the appropriate UV laser. In the meantime, a DOTA derivative will be produced to sensitize the macrocycle to the chelated lanthanide for near-visible excitation.

7.2 B_{12}-enDOTAGd

Although GdDOTA is a current contrast agent for MRI imaging, we propose that a B_{12}-based GdDOTA will be a target-specific bioprobe. Target-specificity of the contrast agent will aid in increasing the sensitivity of the scans for more reliable results. The gadolinium metal can be chelated into the B_{12}-

enDOTA system in a similar reflux as the reactions with europium and terbium, as described in Section 6.

7.3 B_{12}-ReThiazolate

The synthesis, purification, and characterization of a water-soluble (at physiological conditions), rhenium(I)-containing B_{12} bioprobe, B_{12}-ReThiazolate, has recently been established by the author using a similar synthetic scheme to B_{12}-ReBQBA sythesis (Figure 18). This probe will be used in similar applications as the B_{12}-ReBQBA conjugate described in detail in Section 5; however, this water-soluble conjugate solves the solubility issue associated with B_{12}-ReBQBA. This bioprobe will be tested on the T-47D and MIA PaCa-2 cancer cell lines that will be used for the lanthanide imaging work to confirm the presence of certain B_{12} receptors.

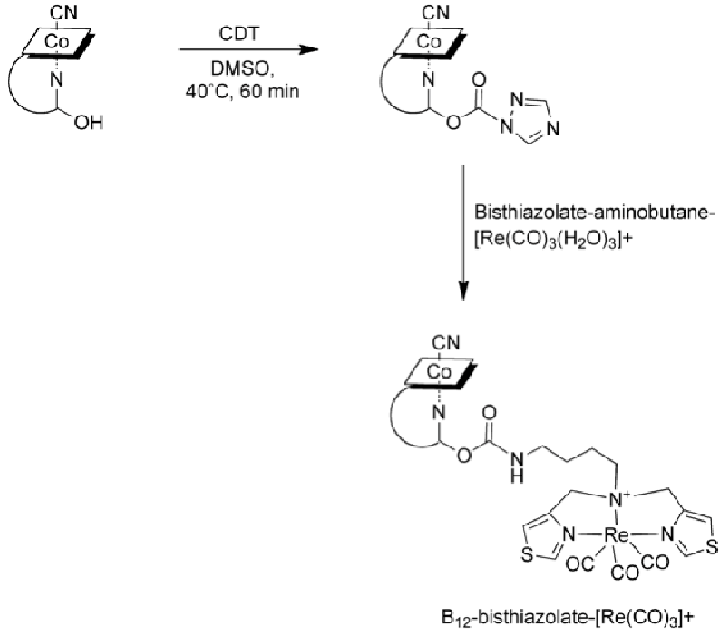

Figure 18. Synthetic scheme for B_{12}-ReThiazolate.

7.4 B_{12}-99mTcBQBA/Thiazolate

The technetium-99m conjugates of the B_{12}-ReBQBA and B_{12}-

ReThiazolate systems will be synthesized for *in vivo* testing. The use of ^{99m}Tc will allow a SPECT scan to be taken of the animal model to determine the biodistribution of the bioprobe with respect to the implanted tumor cells. This biodistribution study will provide insight into the specificity of the bioprobe.

7.5 B_{12}-enDOTA^{64}Cu

In collaboration with the Department of Radiology at Washington University in St. Louis, MO, radioactive copper-64 will be incorporated into the B_{12}-enDOTA construct. The ^{64}Cu labeling will be used first for *in vitro* analysis in the T-47D and MIA PaCa-2 cells to test for uptake. With successful *in vitro* analyses, *in vivo* tests will be performed to determine the biodistribution to the bioprobe with respect to the tumor cells.

7.6 β-Acid Derivative of B_{12}

As a control for the B_{12}-enDOTA studies, a second B_{12}-enDOTA derivative will be synthesized; however, the linker and bifunctional ligand (enDOTA) will be conjugated to the β-amide of B_{12} instead of the 5′ hydroxyl group of the ribose moiety, as represented in Figure 19. Since the β-amide is known to participate in transport protein binding, particularly TCII,

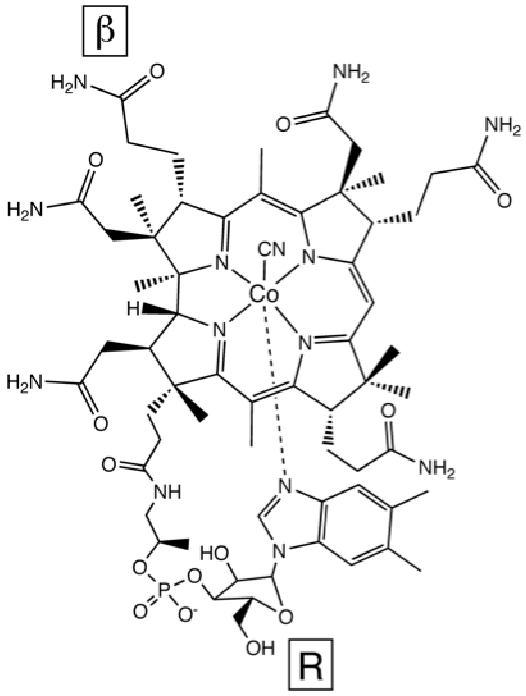

Figure 19. Sites of derivation in B_{12} include the β position, which refers to the β-amide and the R position, which refers to the 5′ hydroxyl group on the ribose moiety).

conjugation through this site will inhibit uptake of the bioprobe in cells that only express the TCII receptor, such as the MIA PaCa-2 cells. This amide group will be converted to an acid group using an acid, such a hydrochloric acid. The β-acid will be purified using anion exchange and C_{18} columns on the RP-HPLC. The correct β-acid will be confirmed using MALDI-TOF/MS and ^{13}C NMR. Once the β-acid is isolated, en will be conjugated to it using EDC and sulfo-NHS activation. DOTA will be conjugated using a similar coupling mechanism. The metal will be chelated to DOTA under reflux conditions. Once purified, the labeled β-acid will be tested on the T-47D and MIA PaCa-2 cell lines. The β-acid bioprobe is expected to be taken into the T-47D cells by HC; however, the bioprobe is only expected to adhere to the cell surface of the MIA PaCa-2 cells due to the presence of TCII and the absence of HC.

8 References

[i] American Cancer Society. *Cancer Facts & Figures 2009.*

[ii] Loeb, K. R.; Loeb, L. A. *Carcinogenesis* **2000**, *21*, 379-385.

[iii] Nakazawa, H.; English, D.; Randell, P. L.; Nakazawa, K.; Martel, N.; Armstrong, B. K.; Yamasaki, H. *Proc. Natl. Acad. Sci. U.S.A.* **1994**, *91*, 360-364.

[iv] Zur Hausen, H. *Nat. Rev. Cancer.* **2002**, *2*, 342-350.

[v] Merlo, L. M. F.; Pepper, J. W.; Reid, B. J.; Maley, C. C. *Nat. Rev. Cancer.* **2006**, *6*, 924-935.

[vi] Stratton, M. R.; Campbell, P. J.; Futreal, P.A. *Nature* **2009**, *458*, 719-24.

[vii] Wooster, R.; Bignell, F.; Lancaster, J.; Swift, S.; Seal, S.; Mangion, J.; Collins, N.; Gregory, S.; Gumbs, C.; Micklem, F.; Barfoot, R.; Hamoudi, R.; Patel, S.; Rice, C.; Biggs, P.; Hashim, Y.; Smith, A.; Connor, F.; Arason, A.; Gunmundsson, J.; Ficenec, D.; Delsell, D.; Ford, D.; Tonin, P.; Bishop, D. T.;

Spurr, N. K.; Ponder, B. A. J.; Eeles, R.; Peto, J.; Devilee, P.; Cornelisse, C.; Lynch, H.; Narod, S.; Lenior, G.; Egilsson, V.; Barkadottir, R.B.; Easton, D. F.; Bentley, D. R.; Futreal, P. A.; Ashworth, A.; Stratton, M. R. *Nature* **1995**, *378*, 789-92.

[viii] Orel, S.; Schnall, M. *Radiology* **2001**, *220*, 13-30.

[ix] Saslow, D.; Boetes, C.; Burke, W.; Harms, S.; Leach, M. O.; Lehman, C. D.; Morris, E.; Pisano, E.; Schnall, M.; Sener, S.; Smith, R. A.; Warner, E.; Yaffe, M.; Andrews, K. S.; Russel, C. A. *CA Cancer J. Clin.* **2007**, *57*, 75-89.

[x] Hinshaw, W. S.; Bottomley, P. A.; Holland, G. N. *Nature* **1977**, *270*, 722-723.

[xi] Jeong, J. M.; Chung, J-K. *Cancer Biother. & Radiopharm.* **2003**, *18*, 707-17.

[xii] Hamblin, J.; Abboyi, N.; Lowe, M. P. *Chem Commun.* **2005**, 657-9.

[xiii] Vitha, T.; Kubícek, V.; Hermann, P.; Elst, L. V.; Muller, R. N.; Kolar, Z. I.; Wolterbeek, H. T.; Breeman, W. A. P.; Lukes, I.; Peters, J. A. *J. Med. Chem.* **2008**, *51*, 677-83.

[xiv] Richardson, F. S. *Chem. Rev.* **1982**, *82*, 541-52.

[xv] McMahon, B.; Mauer, P.; McCoy, C. P.; Clive Lee, T.; Gunnlaugsson, T. *J. Am. Chem. Soc.* **2009**, *131*, 17542-3.

[xvi] Bornhop, D. J.; Griffin, J. M. M.; Goebel, T.S.; Sudduth, M. R.; Bell, B.; Motamedi, M. *Appl. Spectrosc.* **2003**, *57*, 1216-22.

[xvii] Thunus, L.; Lejeune, R. *Coord. Chem. Rev.* **1999**, *184*, 125-55.

[xviii] Russell-Jones, G.; McTavish, K.; McEwan, J.; Rice, J.; Nowotnik, D. *J. Inorg. Biochem.* **2004**, *98*, 1625-33.

[xix] Wang, X., Wei, L.; Kotra, L. P. *Bioorg. Med. Chem.* **2007**, *15*, 1780-87.

[xx] Food and Nutrition Board. *National Academy Press*. **1998**, 306-356.

[xxi] Raux, E.; Zchubert, H. L.; Warren, M. J. *Cell. Mol. Life Sci.* **2000**, *57*, 1880-1893.

[xxii] Wuerges, J.; Garau, G.; Geremia, S.; Fedosov, S. N.; Petersen, T.E.; Randaccio, L. *Proc. Natl. Acad. Sci. U.S.A*. **2006**, *103*, 4386-91.

[xxiii] Stabler, S. P.; Allen, R. H. *Annu. Rev. Nutr.* **2004**, *24*, 299-326.

[xxiv] Baik, H. W.; Russell, R. M. *Annu. Rev. Nutr.* **1999**, *19*, 357-77.

[xxv] Smeltzer, C. C.; Cannon, M. J.; Pinson, P. R.; Munger, Jr., J. D.; West, F. G.; Grissom, C. B. *Org. Lett.* **2001**, *3*, 799-801.

[xxvi] Kunze, S.; Zobi, F.; Kurz, P.; Spingler, B.; Alberto, R. *Angew. Chem. Int. Ed.* **2004**, *43*, 5025-9.

[xxvii] Pathare, P. M.; Wilbur, D. S.; Heusser, S.; Quadros, E. V.; McLoughlin, P.; Morgan, A. C. *Bioconjugate Chem.* **1996**, *7*, 217-232.

[xxviii] Fedosov, S. N.; Grissom, C. B.; Fedosova, N. U.; Moestrup, S. K.; Nexo, E.; Petersen, T. E. *FEBS*. **2006**, *273*, 4742-53.

[xxix] Patillo, R. A.; Gey, G. O.; Delfs, E.; Huang, W. Y.; Hause, L.; Garancis, J.; Knoth, M.; Amatruda, J.; Bertino, J.; Friesen, H. G.; Mattingly, R. F. *Ann. N.Y. Acad. Sci*. **1971**, 172-4.

[xxx] Viola-Villegas, N.; Rabideau, A. E.; Bartholoma, M.; Zubieta, J.; Doyle, R. P. *J. Med. Chem*. **2009**, *52*, 5253-61.

[xxxi] Brasch, N. E.; Finke, R. G. *J. Inorg. Biochem.* **1999**, *73*, 215-9.

[xxxii] Pandya, S.; Yu, J.; Parker, D. *Dalton Trans.* **2006**, 2757-66.